# Thermal Emission of Spinning Photons from Temperature Gradients

P.Y. Chen,[1,*] C. Khandekar,[2] R. Ayash,[1] Z. Jacob,[2] and Y. Sivan[1]

[1] *School of Electrical and Computer Engineering, Ben-Gurion University of the Negev, Be'er Sheva 8410501, Israel*

[2] *School of Electrical and Computer Engineering, Purdue University, West Lafayette, IN 47907, USA*

(Received 14 April 2022; revised 6 May 2022; accepted 26 May 2022; published 21 July 2022)

The fluctuational electrodynamic investigation of thermal radiation from nonequilibrium or nonisothermal bodies remains largely unexplored because it necessarily requires volume integration over the fluctuating currents inside the emitter, which quickly becomes computationally intractable. Here, we put forth a formalism combining fast calculations based on modal expansion and fluctuational electrodynamics to accelerate research at this frontier. We employ our formalism on a sample problem: a long silica wire held under temperature gradient within its cross section. We discover that the far-field thermal emission carries a nonzero spin, which is constant in direction and sign, and interestingly, is transverse to the direction of the power flow. We clearly establish the origin of this transverse spin as arising from the nonequilibrium intermixing of the cylindrical modes of the wire, and not from any previously studied or intuitively expected origins such as chiral or nonisotropic materials and geometries, magnetic materials or fields, and mechanical rotations. This finding of nonequilibrium spin texture of emitted heat radiation can prove useful for advancing the noninvasive thermal metrology or infrared-imaging techniques.

DOI: 10.1103/PhysRevApplied.18.014052

## I. INTRODUCTION

The field of thermal radiation initiated the quantum revolution at the beginning of the twentieth century and spawned numerous technological applications such as thermal energy harvesting, infrared imaging, metrology, gas sensing, and heat management, among others [1–4]. One emerging research direction focuses on the spin angular momentum or circular polarization of thermal radiation. The key guiding principle for this research has been the photon-spin-resolved Kirchhoff's law, which equates emissivity with absorptivity separately for individual circular polarization states of thermally emitted light. However, this law is derived and applicable only to uniform-temperature reciprocal media [5–7]. While recent works have explored the spin angular momentum of thermal radiation from time-reversal-symmetry-broken nonreciprocal media [8–10], it remains an open question whether nonuniform temperature profiles can lead to interesting effects on the circular polarization of thermal emission.

In this work, we develop the theoretical and computational framework to analyze the spin angular momentum of thermal radiation from bodies with nonuniform temperature profiles. As an experimentally relevant example, we consider a long cylindrical rod with a nonuniform temperature distribution across its cross section. Our analysis is performed by extending the recently developed techniques for rapid simulation of Green's function [11–13] to thermal radiation. Crucially, we focus on the spin angular momentum rather than the radiative heat flux. Shown in the left panel of Fig. 1, a long (silica, $SiO_2$) rod is held under a linear temperature gradient. We find that, in the far field, the heat flux is radially outward, but there also exists a nonzero spin-angular-momentum density parallel to the axis of the cylinder and transverse to the emission direction. The left panel also shows the sense of polarization rotation associated with the dimensionless spin, while the right panel displays its magnitude, with blue (red) indicating positive (negative) directionality. With detailed analysis, we prove that this transverse spin is uniquely enabled by the nonuniform temperature distributions and arises from the intermixing of contributions from different cylindrical modes. We also show numerically that the spin magnitude diminishes with diminishing temperature gradient, falling to zero for a uniform temperature profile (Fig. 2).

Until recently, inquiries into the nature of spin arising from thermal radiation were limited to reciprocal media, focusing on two major themes: far-field spin from reciprocal chiral absorbers explored theoretically [14,15] and experimentally [16,17], and the analysis of the degree of polarization in the near field of reciprocal media [18]. Recent exploration of this topic for nonreciprocal media has revealed surprising phenomena, such as persistent

*parryyu@post.bgu.ac.il

 © 2022 American Physical Society

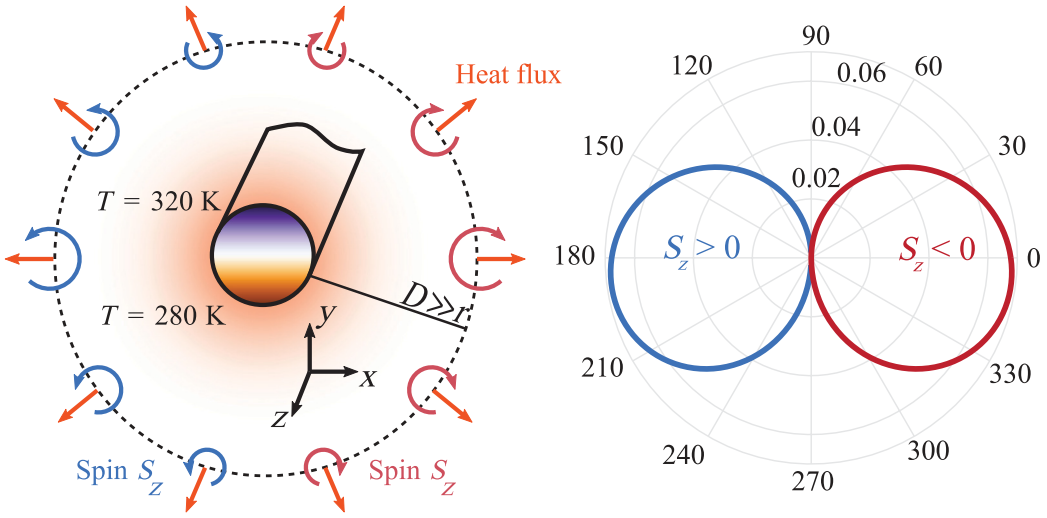


FIG. 1. (Left) An example geometry that can be treated by our formalism for nonequilibrium fluctuation electrodynamics. A temperature gradient is maintained across the cross section of a circular silica rod, which extends infinitely along the $z$ direction. Heat flux, characterized by Poynting's vector, is generated along the radial direction. More notably, spin fields are generated that are in plane, characterized by a spin vector, which is perpendicular to both the plane and the Poynting vector. The circular arrows representing the spin are an artistic depiction rather than an actual indication of its magnitude. (Right) The spin extends into the far field, $D \gg r$, where $r$ is the radius of the cylinder and $D$ is the radius of the far-field contour. The normalized quantity $\langle S_z \rangle \omega / \langle W \rangle$ converges to the displayed nonzero values. The sign and the magnitude of the far-field spin vector changes as a function of the in-plane polar angle, but does not substantially change at scales of the order of the wavelength.

equilibrium spin in the near-field [19] and modified spin-resolved Kirchhoff's laws for planar media [20]. Reference [21] revealed an origin of far-field thermal-radiation spin: a nonequilibrium system composed of a dimer of two coupled antennas held at unequal but uniform or homogeneous temperatures. Along this vein, our work demonstrates a fundamental finding that even nonuniform temperature gradients inside a single thermal emitter can cause thermal emission with a nonzero spin. Our specific example system lacks all previously known aspects connected with the photon spin such as geometric chirality (e.g., nonsymmetrical shapes), material chirality (e.g., chiral or anisotropic materials), magnetic field or magnetic materials, and mechanical rotations. By avoiding these aspects, our work clearly establishes a surprising connection between the nonzero photon spin and the intrinsic temperature gradients. We also note that, in contrast to all previous works reporting longitudinal spin, the far-field spin emitted from the temperature gradient emitter is transverse in nature, thus, making it measurable for greater ease; in fact, such transverse spin was so far believed to be possible only in the near field. We further highlight that the physical origin of this spin is based on nonequilibrium intermixing of cylindrical modes of different orders, which differs from that of Ref. [21], where it stems from the near-field coupling between nonparallel dipole moments.

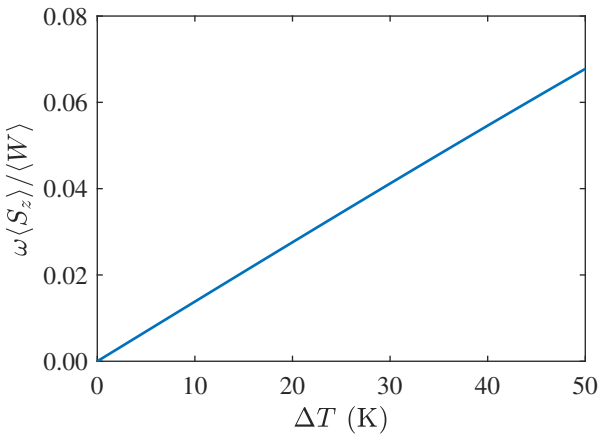


FIG. 2. The magnitude of the far-field spin generated by thermal emission is approximately linearly proportional to the temperature gradient. Along the horizontal axis, the size of $\Delta T$ varies, defined by the hottest and coldest points of the rod in Fig. 3. The vertical axis is the resulting normalized spin density.

Fluctuation-electrodynamic (FE) simulations of thermal radiation from emitters with nonuniform or continuously varying temperature and material profiles necessarily require volume integrals over fluctuating currents, and precludes simplification to surface integrals; the surface current formulations that apply to uniform temperature and material profiles [22–24] are inapplicable here. Note also that there is no Kirchhoff's law for bodies with nonuniform temperature profiles. While Kirchhoff's law can be generalized for differential subvolumes of reciprocal bodies [1], it does not circumvent the need for volume integration for the calculation of the total far-field thermal

radiation spin from such nonisothermal emitters. For volume currents, a formulation was recently developed for emitters with internal inhomogeneities [25], and an alternative approach to tailor the directionality and intensity of thermal emission using temperature gradients was explored in Ref. [26]. These works presented successful but specific numerical techniques. In the present work, we instead aim to develop a general formalism for spatially varying temperature profiles that is compatible with any simulation method. There have been many recent works on thermal radiation in systems of subwavelength particles where the particles can be approximated as point dipoles, thus simplifying the FE simulations and analysis [7,27–29]. Our approach ventures beyond the dipolar regime, paving the way for computationally challenging FE simulations of many-body nondipolar systems.

We employ a modal expansion approach that decomposes the radiation of emitters via their resonator modes. The primary advantage is that once the modes have been obtained using any readily available mode solver, it is computationally inexpensive to analyze the thermal radiation of any temperature profile. This speed is conducive to complex heat-transfer simulations between bodies with nonuniform temperature distributions requiring self-consistent analysis in the presence of other heat-transfer channels like conduction and convection. Furthermore, modal expansion yields useful insights regarding spectral, geometric, and symmetry properties. For example, we can deduce which combination of modes gives rise to nonzero spin simply by considering the spatial overlap between the temperature profile and modal fields. Such insights and design tools are not readily accessible to purely numerical methods such as volume current formulations.

We note that modal expansion was recently used in the form of temporal coupled mode theory (CMT) in Refs. [30,31] to engineer the directionality of Poynting flux. Instead of the eigenfrequency modes employed by CMT, our modal expansion uses eigenpermittivity modes, which offers several advantages. Firstly, eigenpermittivity modes form a discrete set, which is simpler to treat numerically compared with the continuum of frequency modes. Crucially, our formalism can handle temperature inhomogeneities within the spatial extent of a single mode, which is inaccessible to CMT utilizing a single effective mode temperature [30,31]. Furthermore, our formalism is suitable for direct simulation of hybridized or strongly coupled modes in the context of many-body heat-transfer simulations, which for the CMT formalism would require parameter extraction based on numerical fitting beyond the weak-coupling regime. Another advantage of our approach is that the frequencies used for the Planck factor [see Eq. (4) below; the mean energies of an electromagnetic state] are real, thus, avoiding any approximation necessary for complex frequency modes.

## II. FORMULATION

We now develop the formulation for the fields emitted by an arbitrary hot object standing in an optically and thermally uniform background. We assume that the object contains thermal emitters that create a fluctuating current density $\mathbf{J}(\mathbf{r}')$. The total electric and magnetic fields at point $\mathbf{r}$ exterior to the object due to the current $\mathbf{J}(\mathbf{r}')$ are

$$\begin{aligned} E_l(\mathbf{r}) &= ikZ_0 \int d\mathbf{r}' G^E_{lq}(\mathbf{r},\mathbf{r}') J_q(\mathbf{r}'), \\ H_l(\mathbf{r})/Z_0 &= ik \int d\mathbf{r}' G^H_{lq}(\mathbf{r},\mathbf{r}') J_q(\mathbf{r}'), \end{aligned} \tag{1}$$

where $Z_0 = \sqrt{\mu_0/\epsilon_0}$ is the free-space impedance. The electromagnetic properties of the medium are encoded within the Green's tensors.

Our facile yet rigorous treatment of varying temperature profiles is enabled by the expansions

$$\begin{aligned} \bar{\bar{G}}^E(\mathbf{r},\mathbf{r}') &= \frac{1}{k^2} \sum_m \frac{\mathbf{E}^m(\mathbf{r}) \otimes \mathbf{E}^{m,\dagger}(\mathbf{r}')}{\epsilon_m - \epsilon_i}, \\ \bar{\bar{G}}^H(\mathbf{r},\mathbf{r}') &= \frac{1}{k^2} \sum_m \frac{\mathbf{H}^m(\mathbf{r}) \otimes \mathbf{E}^{m,\dagger}(\mathbf{r}')}{\epsilon_m - \epsilon_i}, \end{aligned} \tag{2}$$

where $\epsilon_m$ are the eigenpermittivities associated with the eigenmodes $\mathbf{E}^m(\mathbf{r})$, and $\epsilon_i$ is the permittivity of the object. Notice that the dependence on $\mathbf{r}$ and $\mathbf{r}'$ has been separated into the factors $\mathbf{E}^m(\mathbf{r})$ and $\mathbf{E}^{m,\dagger}(\mathbf{r}')$, a key feature that we later exploit. The above simple form differs from the expansion derived in earlier eigenpermittivity formulations [11,32], since it applies when the source co-ordinate $\mathbf{r}'$ is inside the object. The derivation of electric field part is given in Appendix A, along with a short discussion, and the magnetic field part is obtained using $\bar{\bar{G}}^H(\mathbf{r},\mathbf{r}') = (1/ik)\nabla \times \bar{\bar{G}}^E(\mathbf{r},\mathbf{r}')$. For simplifying later calculations, we also rescale the magnetic field, such that $\mathbf{H} = Z_0 \mathbf{H}^{\mathrm{SI}}$, where $\mathbf{H}^{\mathrm{SI}}$ is the SI quantity.

We employ the fluctuation-dissipation theorem (FDT) [33,34] to calculate the fields produced by ensemble averages of fluctuating currents; products of fluctuating currents are correlated and satisfy

$$\begin{aligned} \langle J_p(\mathbf{r}',\omega') J^*_q(\mathbf{r}'',\omega'') \rangle &= \frac{4\omega\epsilon_0}{\pi} \Theta(\omega,T) \mathrm{Im} \\ &\times [\epsilon(\mathbf{r}')] \delta(\mathbf{r}' - \mathbf{r}'') \delta(\omega' - \omega'') \delta_{pq}, \end{aligned} \tag{3}$$

where

$$\Theta(\omega,T) = \frac{\hbar\omega}{e^{\hbar\omega/k_B T} - 1}, \tag{4}$$

is the mean energy of an electromagnetic state at temperature $T$, and $\langle\rangle$ represents ensemble averaging.

We aim to evaluate various field quantities such as the Poynting flux,

$$\langle P_i(\mathbf{r},\omega)\rangle = \frac{1}{2Z_0}\epsilon_{ilp}\mathrm{Re}\langle E_l^* H_p\rangle, \tag{5}$$

rewritten using tensor notation, with $\epsilon_{ilp}$ being the Levi-Civita symbol for the cross product, and the **H** field is rescaled. Two additional key quantities are the spin momentum density,

$$\langle S_i(\mathbf{r},\omega)\rangle = \frac{\epsilon_{ilp}}{2Z_0 kc^2}\mathrm{Im}\{\langle E_l^* E_p\rangle + \langle H_l^* H_p\rangle\}, \tag{6}$$

and the energy density,

$$\langle W(\mathbf{R},\omega)\rangle = \frac{\delta_{lp}}{2Z_0 c}\{\langle E_l^* E_p\rangle + \langle H_l^* H_p\rangle\}, \tag{7}$$

where $\delta_{lp}$ is the Kronecker $\delta$. Other quantities such as Stokes' parameters can also be considered.

To treat this range of quantities, we consider the general tensor element $\langle D_l^* F_p\rangle$, where $D_l^*$ and $F_p$ can represent either **E** or **H**. The result for cylinders of arbitrary cross section is derived in Appendix B, and is

$$\langle D_l^* F_p\rangle = \frac{2Z_0\epsilon_i''(\omega)}{\pi^2 k}\int_{-k}^{k} d\beta \sum_{m,n} D_l^{m,*}(\mathbf{R})F_p^n(\mathbf{R})\frac{V^{m,n}}{d^{m,n}}, \tag{8}$$

defining the two quantities

$$V^{m,n} = \int d\mathbf{R}'\Theta(\omega,T)\mathbf{E}^{m,\dagger,*}(\mathbf{R}')\cdot\mathbf{E}^{n,\dagger}(\mathbf{R}'), \tag{9}$$

$$d^{m,n} = (\epsilon_m - \epsilon_i)^*(\epsilon_n - \epsilon_i). \tag{10}$$

Equation (8) gives the fields radiated by thermal emission at $\omega$ per unit length of a two-dimensional (2D) geometry standing in free space. As an aside, the equivalent result for three-dimensional (3D) structures is displayed in Eq. (B4). The 3D result is simpler than Eq. (8), as no integration along $\beta$ is necessary since all information pertaining to field profiles is captured by the modes themselves.

The product, Eq. (8), can represent energy flux, Eq. (5), or energy density, Eq. (7), for example. We choose to limit the integral over the longitudinal propagation constant $\beta$ to the propagating Fourier components, see Eq. (B5). The summations over indices $m$ and $n$ run over the same set of modes, as per Eq. (B7). We see that Eq. (8) is composed of three parts. First, the factor $d^{m,n}$ is due to the detuning of the inclusion permittivity $\epsilon_i$ from the eigenpermittivities $\epsilon_m$ of each mode. Second, the integral $V^{m,n}$ over the electric fields of the eigenmodes $\mathbf{E}^{m,\dagger,*}(\mathbf{R}')\cdot\mathbf{E}^{n,\dagger}(\mathbf{R}')$ within the interior of the inclusion is ultimately weighted by the temperature profile. The variable $\mathbf{R} = (x,y)$ ranges over the 2D plane. Finally, the result is given by a sum over the eigenmodal fields $D_l^{m,*}(\mathbf{R})F_p^n(\mathbf{R})$ in the region exterior to the inclusion.

The computational advantage of Eq. (8) is that once the modes of the resonator have been obtained, many quantities of interest regarding the radiation are available by evaluating just the one set of overlap integrals. Even the difficult case of nonuniform temperature profiles can be treated with relative ease. This greatly facilitates any calculation that requires iteration over many temperature profiles, such as self-consistent calculations.

When Eq. (8) is applied to find the Poynting vector, Eq. (5), we obtain

$$\langle \mathbf{P}(\mathbf{R},\omega)\rangle = \frac{\epsilon_i''(\omega)}{\pi^2 k}\int_{-k}^{k} d\beta \sum_{m,n}\mathrm{Re} \times\left\{\mathbf{E}^{m,*}(\mathbf{R})\times\mathbf{H}^n(\mathbf{R})\frac{V^{m,n}}{d^{m,n}}\right\}. \tag{11}$$

The spin momentum density, Eq. (6), is obtained by applying Eq. (8) twice,

$$\langle \mathbf{S}(\mathbf{R},\omega)\rangle = \frac{\epsilon_i''(\omega)}{\pi^2 k^2 c^2}\int_{-k}^{k} d\beta \sum_{m,n}\mathrm{Im} \times\left\{(\mathbf{E}^{m,*}\times\mathbf{E}^n + \mathbf{H}^{m,*}\times\mathbf{H}^n)\frac{V^{m,n}}{d^{m,n}}\right\}. \tag{12}$$

Also, the energy density, Eq. (7), is

$$\langle W(\mathbf{R},\omega)\rangle = \frac{\epsilon_i''(\omega)}{\pi^2 kc}\int_{-k}^{k} d\beta \sum_{m,n}(\mathbf{E}^{m,*}\cdot\mathbf{E}^n + \mathbf{H}^{m,*}\cdot\mathbf{H}^n)\frac{V^{m,n}}{d^{m,n}}. \tag{13}$$

The formalism developed above has been validated against other methods from the literature [35]; see Appendix D.

## III. RESULTS

We use the formalism in Sec. II to treat radiation from a long cylinder with a temperature gradient. Though the geometry is simple, the radiated fields nevertheless exhibit a nontrivial structure. Consider a circular $SiO_2$ rod of radius $r = 4.5$ $\mu$m. We focus on its radiation at a wavelength of 9.4 $\mu$m, where $SiO_2$ is at resonance and has a permittivity of approximately $-3.19 + 4.97i$. The rod rests in a vacuum background at zero temperature. For this geometry, the eigenmodes $\{\mathbf{E}^m\}$ are available analytically (see Ref. [11]), while their eigenvalues $\{\epsilon_m\}$ can be found via a root search [12]. Thus, to use Eq. (8), we need only integrate over $\beta$ and specify a temperature profile. In the results that follow, we integrate over

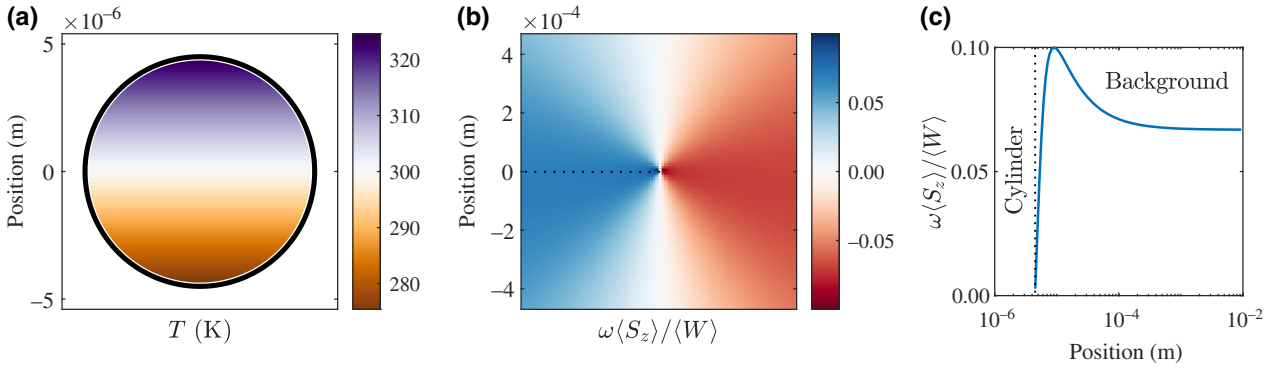


FIG. 3. Emission from a linear temperature gradient. (a) Temperature profile across the cross section of the rod standing in vacuum, featuring the same linear gradient as Fig. 1. (b) Axial spin generated by the radiating rod ($S_z$ normalized by $W$). In this $x$-$y$ plane, there exists a plane of symmetry that coincides with the temperature profile. A different view of the angular variation of $S_z$ is presented in Fig. 1. (c) Axial spin (normalized by $W$), with a strength that does not diminish into the far field; the maximal values of the spin are obtained already about a wavelength away from the rod center, so that the role of the evanescent modes (which are not calculated) are expected to have, at most, a small effect on them. The trajectory for the $x$ axis is along the dotted line of (b) (i.e., $x < 0$, $y = 0$). The plot domain changes drastically across the subfigures.

only the propagating orders, where $\beta < \omega/c$. This means that near fields—within one or two wavelengths of the cylinder—may be inaccurate.

When the cylinder is set to a uniform temperature of 300 K, the cylinder produces rotationally invariant thermal radiation: a Poynting flux oriented in the radial direction. All components of spin are zero, corresponding to the origin of Fig. 2. When a linear temperature gradient is introduced, of the type shown in Fig. 3(a), the profile of the radiated Poynting flux remains largely rotationally invariant (Fig. 5). However, a small but measurable axial component of spin appears, oriented along the $z$ axis (Fig. 1), which is transverse to the radial energy flux. As such, this spin cannot be classified as circular polarization, since the spin axis and Poynting vector do not align. In Fig. 3(b), we plot the spatial profile of this spin, normalized by the energy density, $\langle S_z\rangle\omega/\langle W\rangle$. A plane of symmetry exists in the spin profile, which originates from the symmetry of the temperature profile. However, the sign of the spin is inverted about this plane, since spin is a pseudovector. We also observe in Fig. 3(c) that this spin extends into the far field, where its strength remains undiminished.

These kinds of observations generalize to other temperature gradients. For example, the temperature gradient of Fig. 4(a) contains two planes of symmetry. A nonzero spin is produced [see Fig. 4(b)], containing these two planes of symmetry. Once again, the spin extends into the far field [Fig. 4(c)], but with a smaller magnitude relative to the linear temperature gradient. Crucially, changes to the temperature gradient induce both qualitative and quantitative changes to the far-field spin pattern. By contrast, temperature gradients do not induce any qualitative changes to the far-field Poynting flux, which remains circularly symmetric to zeroth order, as evidenced by Fig. 5. Thus, the far-field spin may enable nondestructive measurement of an emitter's temperature profile.

## IV. DISCUSSION

In this paper, the modal formalism not only provides an efficient means of calculating thermal radiation, especially from spatially varying temperature profiles, but also provides insight into its behavior. For example, we can identify the origins of the nonzero spin, yielding insights into symmetry and spectral properties. From Eq. (12), the spin pattern is determined by products of pairs of modes, each weighted by just two quantities: a geometric factor $V_{mn}$ and a detuning factor $d_{mn}$. The former is the extent to which the modal pair is excited by a particular temperature profile, while the latter is the combined detuning from the resonances of both modes. Finally, the total spin is a sum over all pairs of modes.

We may apply this understanding to the spin radiation patterns of Figs. 3 and 4. In this case, cylindrical symmetry is present, so all modes can be assigned an azimuthal variation $\exp(iM\theta)$, for some integer $M$ corresponding to the angular quantum number. In terms of this cylindrical harmonic basis, we observe that if the temperature profile is uniform, then the geometric factor $V_{mn}$ will always vanish for modal pairs with two different values of $M$. Since two modes with the same $M$ never generate spin when both positive and negative orders are considered, uniform temperature profiles always yield a zero spin field. The same reasoning implies that pure radial gradients of temperature also yield zero spin (not shown).

We now proceed to identify the values of $M$ that do generate spin. In Fig. 3, the spin field resembles $\cos\theta$ to lowest order, and is generated by a combination of modes of orders $M = 0$ and $M = \pm 1$. In Fig. 4, the spin

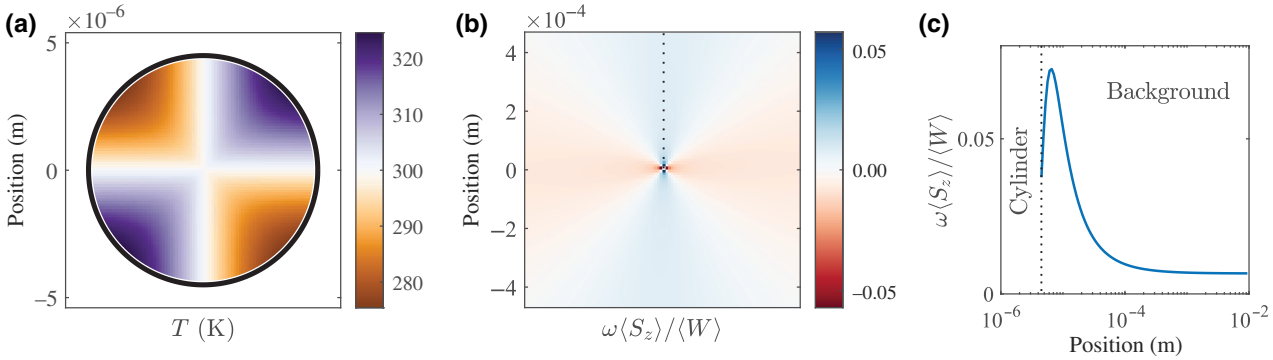


FIG. 4. As in Fig. 3, but with a linear temperature profile with four lobes. (a) Temperature profile over the rod cross section. (b),(c) Axial spin (normalized by $W$).

pattern resembles $\cos 2\theta$, and is generated by modes of orders $M = 1$ and $M = -1$. This difference may mean that the resonance condition for the four-lobe temperature pattern is easier to satisfy, since the resonances of $M = \pm 1$ orders are degenerate. Finally, we may prove that the only component of spin allowed to be nonzero is the $z$ component. This result holds for infinite rods of any cross section and any cross-section temperature profile, and is proven in Appendix C.

## V. OUTLOOK

The modal formalism presented here lays the groundwork for exploring a range of more sophisticated physical scenarios. For example, objects with more complicated shapes (e.g., wires with noncircular cross section, general 3D objects etc.), anisotropy and/or permittivity nonuniformity caused by temperature inhomogeneities [36–38] can be treated using the mode calculation procedure described in Refs. [13,39,40], known as re-expansion; the symmetry consideration discussed above can be used to deduce the necessary temperature uniformity profile for which spin emission can be realized. Our formulation is also applicable to bound modes below the light line in order to determine the correct near-field emission. Together with unique ability of permittivity mode expansion to treat the interactions between multiple objects (see, e.g., Refs. [32,41,42]), this allows the thermal emission from multiple interacting structures to be treated, and would be crucial for accurate modeling of near-field heat transfer (see Ref. [43]). It would also be an efficient building block in inverse design algorithms aimed at optimizing thermal emission. Finally, our formulation can also be applied to other computationally heavy problems, such as Förster energy transfer, quantum friction, and Casimir forces.

The spin emitted by the temperature gradient that we consider is transverse to the Poynting vector. It cannot be measured by traditional approaches based on quarter-wave plates, which is only suitable for the measurement of longitudinal spin. Therefore, the experimental detection of such transverse spin would require alternative approaches such as the one recently proposed for measuring photonic spin density using N-$V$ centers [44] or by measuring the resulting torque on levitating nanoparticles [45]. The central result of this work has practical implications for situations requiring noncontact depth thermography

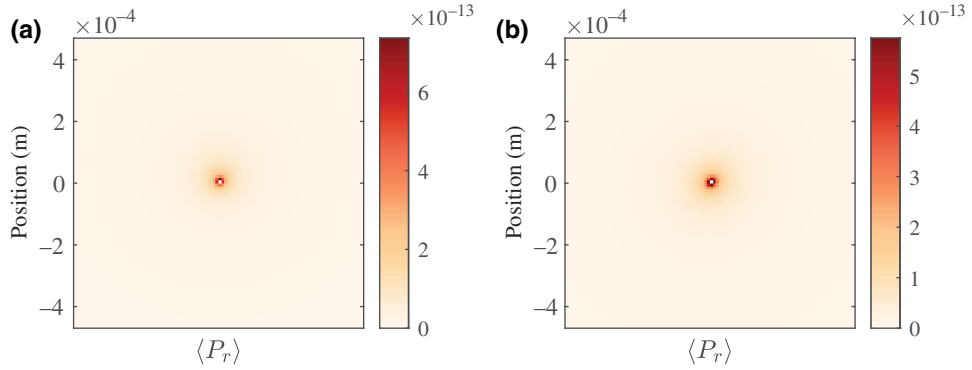


FIG. 5. The radial flux associated with the temperature profiles of (a) Fig. 3 and (b) Fig. 4. The difference of the Poynting flux produced by the two temperature profiles is quantitative rather than qualitative. For example, no other nodes are introduced when the symmetry of the temperature profile is changed.

(temperature measurement) based on emitted IR radiation. By comparing the experimental measurements of spin over different emission directions and prior simulation studies (made faster by our modal expansion approach) of the same for various temperature gradient profiles, one can potentially deduce gradient directions. In other words, measurement of photon spin in addition to thermal radiation power can provide valuable additional insight for nanoscale temperature metrology. Fundamentally, the connection between thermal nonequilibria and photon spin is nonintuitive and remains an exciting, unexplored research area.

## ACKNOWLEDGMENTS

The authors thank N. Shitrit for fruitful and illuminating discussions. The authors acknowledge funding from the DARPA NLM program.

## APPENDIX A: GENERALIZED NORMAL MODE EXPANSION (GENOME) OF GREEN'S TENSOR

The electromagnetic Green's tensor $\bar{\bar{G}}(\mathbf{r},\mathbf{r}')$ gives the field radiated by a classical dipole of any orientation at a given distance away from the source,

$$\nabla\times(\nabla\times\bar{\bar{G}})-k^2\epsilon(\mathbf{r})\bar{\bar{G}}=\bar{\bar{I}}\delta^3(\mathbf{r}-\mathbf{r}'), \tag{A1}$$

where $\mathbf{r}$ and $\mathbf{r}'$ are the locations of the detector and source. The radiation occurs at frequency $\omega=ck$ in the presence of a structure defined by $\epsilon(\mathbf{r})$. The Green tensor of a closed resonator can be expanded using the normal modes of the resonator, often capturing its behavior with just a few eigenmodes.

In Ref. [11], a modal expansion of Green's tensor was developed for open systems. Its most notable feature is its use of true stationary states, which are more suitable for simulations at real frequencies. For this reason, it was named GEneralized Normal-Mode Expansion (GENOME), as it recovers the simplicity and rigour of normal-mode expansion for closed systems. The generalized normal modes are based on the Lippmann-Schwinger equation, a commonly used formalism for scattering calculations in many areas of physics. It can be derived from Maxwell's equations in the presence of a source distribution $\mathbf{J}$,

$$\nabla\times(\nabla\times\mathbf{E})-k^2\epsilon(\mathbf{r})\mathbf{E}=i\omega\mu_0\mathbf{J}, \tag{A2}$$

where we assume nonmagnetic media and harmonic $e^{-i\omega t}$ time variation. By assuming that the structure rests in a uniform background of permittivity $\epsilon_b$, its response can be split from the $k^2\epsilon(\mathbf{r})\mathbf{E}$ term and moved to the right-hand side to yield the differential form of the Lippmann-Schwinger equation,

$$\nabla\times(\nabla\times\mathbf{E})-k^2\epsilon_b\mathbf{E}=k^2(\epsilon(\mathbf{r})-\epsilon_b)\mathbf{E}+i\omega\mu_0\mathbf{J}. \tag{A3}$$

For simplicity, we assume that the inclusion is of uniform permittivity $\epsilon_i$, simplifying the term on the right hand side to $k^2(\epsilon_i-\epsilon_b)\theta(\mathbf{r})\mathbf{E}$. The shape of the inclusion is encoded by the indicator function $\theta(\mathbf{r})$, which equals one inside the inclusion and is zero outside. Nonuniform inclusions [39] and inclusions with tensorial permittivities [13] can also be treated, and the following formulation can readily be generalized using the references provided.

An eigenvalue equation can then be defined for the generalized normal modes by setting sources $\mathbf{J}$ to zero

$$\nabla\times(\nabla\times\mathbf{E}^m)-k^2\epsilon_b\mathbf{E}^m=s_m k^2\theta(\mathbf{r})\mathbf{E}^m, \tag{A4}$$

where we have furthermore assumed that the inclusion is of uniform permittivity. The eigenvalue $s_m$ corresponds to the permittivity $\epsilon_m$ of the inclusion, which brings the system, Eq. (A4), to resonance,

$$s_m\equiv\frac{\epsilon_b}{\epsilon_b-\epsilon_m}. \tag{A5}$$

The eigenvalue equation (A4) can be solved analytically for simple geometries such as cylinders, yielding a transcendental equation for eigenvalues. Efficient and reliable root search procedures are available for these equations [12].

We now formulate the expansion of Green's tensor, Eq. (2), using the generalized normal modes, Eq. (A4). We expand $\bar{\bar{G}}(\mathbf{r},\mathbf{r}')$ via

$$\bar{\bar{G}}(\mathbf{r},\mathbf{r}')=\sum_m\mathbf{E}^m(\mathbf{r})\otimes\gamma^{\mathbf{m}}(\mathbf{r}'), \tag{A6}$$

where $\gamma^{\mathbf{m}}(\mathbf{r}')$ are as yet unknown coefficients that depend on the source location $\mathbf{r}'$. The procedure for evaluating these unknowns begins by inserting Eq. (A6) into Eq. (2) so that

$$\sum_m[\nabla\times(\nabla\times\mathbf{E}^m(\mathbf{r}))-k^2\epsilon_b\mathbf{E}^m(\mathbf{r}) - k^2\theta(\mathbf{r})(\epsilon_i-\epsilon_b)\mathbf{E}^m(\mathbf{r})]\otimes\gamma^m(\mathbf{r}')=\bar{\bar{I}}\delta^3(\mathbf{r}-\mathbf{r}'). \tag{A7}$$

This can be simplified using the defining equation for the eigenmodes, Eq. (A4), to yield

$$k^2\sum_m(\epsilon_m-\epsilon_i)\theta(\mathbf{r})\mathbf{E}^m(\mathbf{r})\otimes\gamma^{\mathbf{m}}(\mathbf{r}')=\bar{\bar{I}}\delta^3(\mathbf{r}-\mathbf{r}'). \tag{A8}$$

The unknowns can then be found by projecting onto an adjoint mode $\mathbf{E}^{n,\dagger}(\mathbf{r})$,

$$k^2 \sum_m (\epsilon_m - \epsilon_i) \left\{ \int \mathbf{E}^{n,\dagger}(\mathbf{r}) \cdot \theta(\mathbf{r}) \mathbf{E}^m(\mathbf{r}) dr \right\} \gamma^{\mathbf{m}}(\mathbf{r}') = \int \mathbf{E}^{m,\dagger}(\mathbf{r}) \delta^3(\mathbf{r} - \mathbf{r}') d\mathbf{r}', \tag{A9}$$

and simplifying using the orthonormality relation between modes,

$$\int \mathbf{E}^{n,\dagger}(\mathbf{r}) \cdot \theta(\mathbf{r}) \mathbf{E}^m(\mathbf{r}) dr = \delta_{nm}. \tag{A10}$$

This relation has been proven elsewhere [11]. By inserting $\gamma^m(\mathbf{r}')$ back into Eq. (A6), we obtain the desired expansion, Eq. (2). Note the similarity of this expression to the quasinormal mode expansion of Green's tensor [46].

This expression is valid for our purposes, where the source is inside the inclusion. When the source $\mathbf{r}'$ is located in the background, a slightly more complex expression is necessary [11]. In that expansion, the divergence of Green's function at the source location is completely represented by a separate term. However, this separate term is not necessary for our purposes here, since all sources are interior to the resonator, where the set of eigenpermittivity modes are complete.

## APPENDIX B: DERIVATION OF EMITTED FIELDS

We aim to calculate the tensor component $\langle D_l^* F_p \rangle$, consisting of a product of two fields, defined in Eq. (8). We begin by inserting a generalized form of Eq. (1),

$$\begin{aligned} \langle D_l^* F_p \rangle &= \left\langle \left[ ikZ_0 \int d\mathbf{r}' G_{lq}^D(\mathbf{r}, \mathbf{r}') J_q(\mathbf{r}') \right]^* \left[ ikZ_0 \int d\mathbf{r}'' G_{po}^F(\mathbf{r}, \mathbf{r}'') J_o(\mathbf{r}'') \right] \right\rangle \\ &= k^2 Z_0^2 \iint d\mathbf{r}' d\mathbf{r}'' G_{lq}^{D,*}(\mathbf{r}, \mathbf{r}') G_{po}^F(\mathbf{r}, \mathbf{r}'') \langle J_q^*(\mathbf{r}') J_o(\mathbf{r}'') \rangle. \end{aligned} \tag{B1}$$

Thus, the field product reduces to

$$\langle D_l^* F_p \rangle = \frac{4k^3 Z_0 \epsilon_i''(\omega)}{\pi} \int d\mathbf{r}' \Theta(\omega, T) G_{lq}^{D,*}(\mathbf{r}, \mathbf{r}') G_{pq}^F(\mathbf{r}, \mathbf{r}'), \tag{B2}$$

assuming that the imaginary part of permittivity $\epsilon_i''$ remains uniform in the interior. At this point, we insert a generalized form of Eq. (2),

$$G_{lq}^F(\mathbf{r}, \mathbf{r}') = \frac{1}{k^2} \sum_m \frac{F_l^m(\mathbf{r}) E_q^{m,\dagger}(\mathbf{r}')}{\epsilon_m - \epsilon_i}, \tag{B3}$$

where $F$ can represent either the electric or magnetic field. This yields

$$\begin{aligned} \langle D_l^* F_p \rangle &= \frac{4Z_0 \epsilon_i''(\omega)}{k\pi} \int d\mathbf{r}' \Theta(\omega, T) \sum_m \sum_n \frac{D_l^{m,*}(\mathbf{r}) E_q^{n,\dagger,*}(\mathbf{r}')}{\epsilon_m^* - \epsilon_i^*} \frac{F_p^n(\mathbf{r}) E_q^{n,\dagger}(\mathbf{r}')}{\epsilon_n - \epsilon_i} \\ &= \frac{4Z_0 \epsilon_i''(\omega)}{k\pi} \sum_{m,n} D_l^{m,*}(\mathbf{r}) F_p^n(\mathbf{r}) \frac{\int d\mathbf{r}' \Theta(\omega, T) E_q^{n,\dagger,*}(\mathbf{r}') E_q^{n,\dagger}(\mathbf{r}')}{(\epsilon_m - \epsilon_i)^* (\epsilon_n - \epsilon_i)}, \end{aligned} \tag{B4}$$

which concludes the derivation for 3D geometries.

In the main text, our numerical examples feature 2D inclusions with infinite translational symmetry along one direction. In this case, the formulation differs from Eq. (B4). For this derivation, we return to Eq. (B2), and take the Fourier transform along the $z$ direction. We orient this direction along $z$, while the in-plane coordinates are denoted by $\mathbf{R} = (x, y)$. In this case, the 3D Green tensor is

related to the 2D Green tensor, $\bar{\bar{G}}^{2D}(\mathbf{R},\mathbf{R}',\beta)$,

$$G^F_{lq}(\mathbf{r},\mathbf{r}') = \frac{1}{2\pi}\int_{-k}^{k} d\beta\, e^{i\beta(z-z')} G^{F,2D}_{lq}(\mathbf{R},\mathbf{R}',\beta). \quad \text{(B5)}$$

Since we are interested in the radiation into the far field, we can limit the range of integration of $\beta$ to the light cone, i.e., from $-\omega/c$ to $\omega/c$. We proceed with

$$\begin{aligned}\langle D^*_l F_p\rangle &= \frac{4k^3 Z_0 \epsilon_i''(\omega)}{\pi}\int d\mathbf{r}'\Theta(\omega,T) G^{D,*}_{lq}(\mathbf{r},\mathbf{r}') G^F_{pq}(\mathbf{r},\mathbf{r}')\\ &= \frac{4k^3 Z_0 \epsilon_i''(\omega)}{\pi}\iint d\mathbf{R}'dz'\Theta(\omega,T)\int_{-k}^{k}\int_{-k}^{k}\frac{d\beta d\beta'}{(2\pi)^2}\\ &\quad\times e^{i(\beta'-\beta)(z-z')} G^{D,2D,*}_{lq}(\mathbf{R},\mathbf{R}',\beta) G^{F,2D}_{pq}(\mathbf{R},\mathbf{R}',\beta')\\ &= \frac{4k^3 Z_0 \epsilon_i''(\omega)}{\pi}\int d\mathbf{R}'\Theta(\omega,T)\int_{-k}^{k}\frac{d\beta}{2\pi} G^{D,2D,*}_{lq}\\ &\quad\times(\mathbf{R},\mathbf{R}',\beta) G^{F,2D}_{pq}(\mathbf{R},\mathbf{R}',\beta)\\ &= \frac{2k^3 Z_0 \epsilon_i''(\omega)}{\pi^2}\int_{-k}^{k} d\beta\int d\mathbf{R}'\Theta(\omega,T) G^{D,2D,*}_{lq}\\ &\quad\times(\mathbf{R},\mathbf{R}',\beta) G^{F,2D}_{pq}(\mathbf{R},\mathbf{R}',\beta). \end{aligned} \quad \text{(B6)}$$

We assume that the temperature profile is not a function of $z'$, so the integration over $z'$ allows the elimination of the integral over $\beta'$.

To complete the derivation, we need to use the specific expansions of 2D Green tensors in terms of the generalized normal modes (2), which in generalized form reads

$$G^{F,2D}_{lq}(\mathbf{R},\mathbf{R}',\beta) = \frac{1}{k^2}\sum_m \frac{F^m_l(\mathbf{R}) E^{m,\dagger}_q(\mathbf{R}')}{\epsilon_m - \epsilon_i}. \quad \text{(B7)}$$

The expansion, Eq. (B7), is identical to Eq. (B3), meaning that the same expression applies in 2D and 3D. The only distinction is whether the constituent modes are 2D or 3D. We have also suppressed the $\beta$ dependence on the right-hand side for brevity. As a side note, this is always a sum over a discrete set in the GENOME expansion, even for the radiating modes that we considered in Eq. (B5). This is one of the advantages of designating permittivity to be the eigenvalue. Finally, we substitute this generalized form into Eq. (B6) to give

$$\begin{aligned}\langle D^*_l F_p\rangle &= \frac{2Z_0\epsilon_i''(\omega)}{\pi^2 k}\int_{-k}^{k} d\beta\int d\mathbf{R}'\Theta(\omega,T)\sum_m\sum_n\\ &\quad\times\frac{D^{m,*}_l(\mathbf{R}) E^{m,\dagger,*}_q(\mathbf{R}')}{\epsilon^*_m - \epsilon^*_i}\frac{F^n_p(\mathbf{R}) E^{n,\dagger}_q(\mathbf{R}')}{\epsilon_n - \epsilon_i}\\ &= \frac{2Z_0\epsilon_i''(\omega)}{\pi^2 k}\int_{-k}^{k} d\beta\sum_{m,n} D^{m,*}_l(\mathbf{R}) F^n_p(\mathbf{R})\\ &\quad\times\frac{\int d\mathbf{R}'\Theta(\omega,T)\mathbf{E}^{m,\dagger,*}(\mathbf{R}')\cdot\mathbf{E}^{n,\dagger}(\mathbf{R}')}{(\epsilon_m-\epsilon_i)^*(\epsilon_n-\epsilon_i)}. \end{aligned} \quad \text{(B8)}$$

## APPENDIX C: SYMMETRY AND NONZERO COMPONENTS

We assume that the structure and temperature profiles in this paper possess certain symmetries, which compels certain components of the thermal fields to be zero. In particular, Eq. (8) and all subsequent results assume that both the rod and the temperature profile are invariant along the infinite $z$ direction. However, no assumptions are made regarding the cross-section profiles of the rod or of temperature. Nevertheless, this forces the $z$ component of the Poynting flux $\mathbf{P}$ to be zero, and the only component of spin $\mathbf{S}$ allowed to be nonzero is the $z$ component.

The proof of these statements begins by noticing that the integrals in Eqs. (11) and (12) run over both positive and negative $\beta$ values, so cancellation occurs if a given quantity is antisymmetric with respect to $\beta$. A mode associated with $\beta$ is the mirror image of the corresponding mode at $-\beta$, specifically a reflection about the $x$-$y$ plane. This means that the $E_z$ component of every mode flips sign, while $E_x$ and $E_y$ do not. Meanwhile, $H_z$ remains invariant under this reflection, while $H_x$ and $H_y$ do change sign, since magnetic fields are pseudovectors. The components of adjoint and complex conjugated modes also behave the same way under reflection.

We may apply this knowledge to deduce that the $z$ component of $\mathbf{P}$ must be zero by symmetry. The integrand in Eq. (11) is comprised of three components: $d^{m,n}$, $V^{m,n}$, and $\mathbf{E}^{m,*}(\mathbf{R})\times\mathbf{H}^n(\mathbf{R})$. Firstly, $d^{m,n}$ is a scalar, and is invariant under reflection. Secondly, the quantity $V^{m,n}\propto\mathbf{E}^{m,\dagger,*}\cdot\mathbf{E}^{n,\dagger}$ is also invariant, since it is composed of products such as $E^{m,\dagger,*}_x E^{n,\dagger}_x$ where both components remain invariant, or the product $E^{m,\dagger,*}_z E^{n,\dagger}_z$, which also remains invariant because both its components acquire a minus sign. Since these two quantities are invariant under reflection, the symmetry properties of $\mathbf{P}$ is entirely determined by $\mathbf{E}^{m,*}(\mathbf{R})\times\mathbf{H}^n(\mathbf{R})$. An analysis of its components reveals that its $r$ and $\theta$ components are invariant as $\beta\to-\beta$, so reflection symmetry does not impose any restrictions on these components. However, $z$ component changes sign as $\beta\to-\beta$, so the

two contributions cancel and the $z$ component of $\mathbf{P}$ must be zero by symmetry.

Similar arguments can be applied to show that only the $z$ component of $\mathbf{S}$ is allowed to be nonzero by symmetry. From Eq. (12), the integrand of $\mathbf{S}$ also consists of the two invariant quantities $d^{m,n}$ and $V^{m,n}$. So $\mathbf{S}$ is determined by the symmetry properties of $\mathbf{E}^{m,*} \times \mathbf{E}^{n} + \mathbf{H}^{m,*} \times \mathbf{H}^{n}$, which can be analyzed as described above.

## APPENDIX D: VALIDATION OF THE METHOD

In the case of a circular cylinder, we may validate our results with analytic results from the published literature [35]. Such results were obtained in a very different way, via the reciprocity theorem and also cylindrical Mie theory, and so offers a suitable comparison. This geometry also possesses infinite rotational symmetry, and the fields of the eigenmode equation (A4) are available analytically, while the eigenvalues can be found via a root search [12].

For a detailed comparison, we consider the individual Fourier components of the radiated energy at a single frequency. In other words, we integrate the radiated power (11) over all radiation directions,

$$\Phi(\omega) = \oint d\hat{\mathbf{n}} \cdot \langle \mathbf{P}(\mathbf{R}, \omega) \rangle = \frac{\epsilon_i''(\omega)}{\pi^2 k} \int_{-k}^{k} d\beta \; \Phi_\beta(\omega), \tag{D1}$$

where $\hat{\mathbf{n}}$ is the unit normal to a closed contour in the 2D plane in $\mathbf{R}$. Here, $\Phi_\beta(\omega)$ is proportional to the power from all modes at a given $\beta$ and $\omega$. We thus plot the integrand in Eq. (D1) along with its leading factors, i.e., $\epsilon_i''(\omega)\Phi_\beta(\omega)/\pi^2 k$. Note that the integral of $\Phi(\omega)$ over all frequencies gives the power emitted per unit length of the cylinder, so $\Phi(\omega)$ has units of $\mathrm{Wsm}^{-1}$.

As a specific example, we calculate the emission at a single wavelength from a cylinder of permittivity $\epsilon = 4.785 + 0.011i$ at temperature $T = 300$ K placed in a 0 K vacuum background. The radius of the cylinder as a ratio of the wavelength is $2\pi a/\lambda = 0.35$. In Fig. 6, we plot results for all propagation constants $\beta$ from 0 to $k = \omega/c$. The results are seen to agree well with the previously published result.

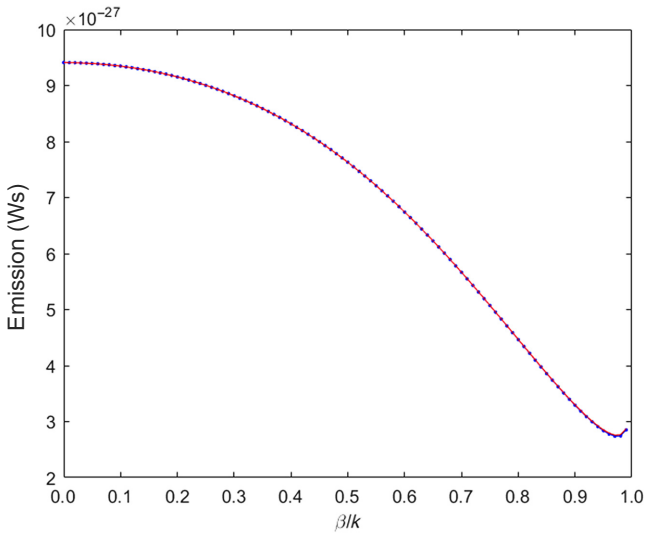


FIG. 6. Emission from a uniform temperature gradient, as a function of the propagation constant $\beta$ along the cylinder axis. The result is calculated in two different ways: using the formalism developed in this paper (blue line with dots) and the method of Ref. [35] based on the reciprocity theorem (red line).


[1] J.-J. Greffet, P. Bouchon, G. Brucoli, and F. Marquier, Light Emission by Nonequilibrium Bodies: Local Kirchhoff Law, Phys. Rev. X **8**, 021008 (2018).

[2] D. A. B. Miller, L. Zhu, and S. Fan, Universal modal radiation laws for all thermal emitters, Proc. Natl. Acad. Sci. USA **114**, 4336 (2017).

[3] W. Li and S. Fan, Nanophotonic control of thermal radiation for energy applications, Opt. Express **26**, 15995 (2018).

[4] D. G. Baranov, Y. Xiao, I. A. Nechepurenko, A. Krasnok, Andrea Alú, and M. A. Kats, Nanophotonic engineering of far-field thermal emitters, Nat. Mater. **18**, 920 (2019).

[5] J.-J. Greffet and M. Nieto-Vesperinas, Field theory for generalized bidirectional reflectivity: Derivation of Helmholtz's reciprocity principle and Kirchhoff's law, JOSA A **15**, 2735 (1998).

[6] A. Resnick, C. Persons, and G. Lindquist, Polarized emissivity and Kirchhoff's law, Appl. Opt. **38**, 1384 (1999).

[7] S.-A. Biehs and P. Ben-Abdallah, Revisiting super-Planckian thermal emission in the far-field regime, Phys. Rev. B **93**, 165405 (2016).

[8] R. M. Abraham Ekeroth, A. García-Martín, and J. C. Cuevas, Thermal discrete dipole approximation for the description of thermal emission and radiative heat transfer of magneto-optical systems, Phys. Rev. B **95**, 235428 (2017).

[9] L. Zhu, Y. Guo, and S. Fan, Theory of many-body radiative heat transfer without the constraint of reciprocity, Phys. Rev. B **97**, 094302 (2018).

[10] X. Gao, C. Khandekar, Z. Jacob, and T. Li, Thermal equilibrium spin-torque: Near-field radiative angular momentum transfer in magneto-optical media, Phys. Rev. B **103**, 125424 (2021).

[11] P. Y. Chen, D. J. Bergman, and Y. Sivan, Generalizing Normal Mode Expansion of Electromagnetic Green's Tensor to Lossy Resonators in Open Systems, Phys. Rev. Appl. **11**, 044018 (2019).

[12] P. Y. Chen and Y. Sivan, Robust location of optical fiber modes via the argument principle method, Comput. Phys. Commun. **214**, 105 (2017).

[13] N. Kossowski, P. Y. Chen, Q. J. Wang, P. Genevet, and Y. Sivan, Generalized normal modes of an anisotropic scatterer, J. Appl. Phys. **129**, 113104 (2021).

[14] C. Wu, N. Arju, G. Kelp, J. A. Fan, J. Dominguez, E. Gonzales, E. Tutuc, I. Brener, and G. Shvets, Spectrally

selective chiral silicon metasurfaces based on infrared Fano resonances, Nat. Commun. **5**, 1 (2014).

[15] S. A. Dyakov, V. A. Semenenko, N. A. Gippius, and S. G. Tikhodeev, Magnetic field free circularly polarized thermal emission from a chiral metasurface, Phys. Rev. B **98**, 235416 (2018).

[16] S. L. Wadsworth, P. G. Clem, E. D. Branson, and G. D. Boreman, Broadband circularly-polarized infrared emission from multilayer metamaterials, Opt. Mater. Express **1**, 466 (2011).

[17] N. Shitrit, I. Yulevich, E. Maguid, D. Ozeri, D. Veksler, V. Kleiner, and E. Hasman, Spin-optical metamaterial route to spin-controlled photonics, Science **340**, 724 (2013).

[18] T. Setälä, M. Kaivola, and A. T. Friberg, Degree of Polarization in Near Fields of Thermal Sources: Effects of Surface Waves, Phys. Rev. Lett. **88**, 123902 (2002).

[19] C. Khandekar and Z. Jacob, Thermal spin photonics in the near-field of nonreciprocal media, New J. Phys. **21**, 103030 (2019).

[20] C. Khandekar, F. Khosravi, Z. Li, and Z. Jacob, New spin-resolved thermal radiation laws for nonreciprocal bianisotropic media, New J. Phys. **22**, 123005 (2020).

[21] C. Khandekar and Z. Jacob, Circularly Polarized Thermal Radiation from Nonequilibrium Coupled Antennas, Phys. Rev. Appl. **12**, 014053 (2019).

[22] A. W. Rodriguez, M. T. H. Reid, and S. G. Johnson, Fluctuating-surface-current formulation of radiative heat transfer: Theory and applications, Phys. Rev. B **88**, 054305 (2013).

[23] G. Bimonte, T. Emig, M. Kardar, and M. Krüger, Nonequilibrium fluctuational quantum electrodynamics: Heat radiation, heat transfer, and force, Annu. Rev. Condens. Matter Phys. **8**, 119 (2017).

[24] M. Krüger, G. Bimonte, T. Emig, and M. Kardar, Trace formulas for nonequilibrium Casimir interactions, heat radiation, and heat transfer for arbitrary objects, Phys. Rev. B **86**, 115423 (2012).

[25] A. G. Polimeridis, M. T. H. Reid, W. Jin, S. G. Johnson, J. K. White, and A. W. Rodriguez, Fluctuating volume-current formulation of electromagnetic fluctuations in inhomogeneous media: Incandescence and luminescence in arbitrary geometries, Phys. Rev. B **92**, 134202 (2015).

[26] W. Jin, A. G. Polimeridis, and A. W. Rodriguez, Temperature control of thermal radiation from composite bodies, Phys. Rev. B **93**, 121403 (2016).

[27] P. Ben-Abdallah, S.-A. Biehs, and K. Joulain, Many-Body Radiative Heat Transfer Theory, Phys. Rev. Lett. **107**, 114301 (2011).

[28] A. Manjavacas and F. J. G. de Abajo, Radiative heat transfer between neighboring particles, Phys. Rev. B **86**, 075466 (2012).

[29] S. Sanders, L. Zundel, W. J. M. Kort-Kamp, D. A. R. Dalvit, and A. Manjavacas, Near-Field Radiative Heat Transfer Eigenmodes, Phys. Rev. Lett. **126**, 193601 (2021).

[30] L. Zhu, S. Sandhu, C. Otey, S. Fan, M. B. Sinclair, and T. S. Luk, Temporal coupled mode theory for thermal emission from a single thermal emitter supporting either a single mode or an orthogonal set of modes, Appl. Phys. Lett. **102**, 103104 (2013).

[31] M. Zhou, E. Khoram, D. Liu, B. Liu, S. Fan, M. L. Povinelli, and Z. Yu, Self-focused thermal emission and holography realized by mesoscopic thermal emitters, ACS Photonics **8**, 497 (2021).

[32] D. J. Bergman and D. Stroud, Theory of resonances in the electromagnetic scattering by macroscopic bodies, Phys. Rev. B **22**, 3527 (1980).

[33] L. Novotny and B. Hecht, *Principles of Nano-Optics* (Cambridge University Press, Cambridge, 2006).

[34] L. A. Sphaier, J. Su, R. M. Cotta, and F. A. Kulacki, *Handbook of Thermal Science and Engineering* (Springer, Cham, Switzerland, 2017).

[35] V. A. Golyk, M. Krüger, and M. Kardar, Heat radiation from long cylindrical objects, Phys. Rev. E **85**, 046603 (2012).

[36] P.-T. Shen, Y. Sivan, C.-W. Lin, H.-L. Liu, C.-W. Chang, and S.-W. Chu, Temperature- and roughness-dependent permittivity of annealed/unannealed gold films, Opt. Exp. **24**, 19254 (2016).

[37] I. Gurwich and Y. Sivan, A metal nanosphere under intense continuous wave illumination: A unique case of non-perturbative nonlinear nanophotonics, Phys. Rev. E **96**, 012212 (2017).

[38] I. W. Un and Y. Sivan, The thermo-optic nonlinearity of single metal nanoparticles under intense continuous-wave illumination, Phys. Rev. Mater. **4**, 105201 (2020).

[39] P. Y. Chen, Y. Sivan, and E. A. Muljarov, An efficient solver for the generalized normal modes of non-uniform open optical resonators, J. Comput. Phys. **422**, 109754 (2020).

[40] P. Y. Chen and Y. Sivan, Resolving Gibbs phenomenon via a discontinuous basis in a mode solver for open optical systems, J. Comput. Phys. **429**, 110004 (2021).

[41] C. Forestiere, G. Miano, G. Rubinacci, A. Tamburrino, R. Tricarico, and S. Ventre, Volume integral formulation for the calculation of material independent modes of dielectric scatterers, IEEE Trans. Antennas Propag. **66**, 2505 (2018).

[42] G. Rosolen, P. Y. Chen, B. Maes, and Y. Sivan, Overcoming the bottleneck for quantum computations of complex nanophotonic structures: Purcell and Förster resonant energy transfer calculations using a rigorous mode-hybridization method, Phys. Rev. B **101**, 155401 (2020).

[43] S. A. Biehs, R. Messina, P. S. Venkataram, J. C. Cuevas, A. W. Rodriguez, and P. Ben-Abdallah, Near-field radiative heat transfer in many-body systems, Rev. Mod. Phys. **93**, 025009 (2021).

[44] F. Kalhor, L.-P. Yang, L. Bauer, and Z. Jacob, Quantum sensing of photonic spin density using a single spin qubit, Phys. Rev. Res. **3**, 043007 (2021).

[45] J. Ahn, Z. Xu, J. Bang, P. Ju, X. Gao, and T. Li, Ultrasensitive torque detection with an optically levitated nanorotor, Nat. Nanotechnol. **15**, 89 (2020).

[46] P. Lalanne, W. Yan, K. Vynck, C. Sauvan, and J.-P. Hugonin, Light interaction with photonic and plasmonic resonances, Lasers Photonics Rev. **12**, 1700113 (2017).